JOURNAL OF COMPUTATIONAL PHYSICS 111, 237–247 (1994)

Extension of the Streamlined Darwin Model to Quasineutral Plasmas

GREGORY DIPESO, DENNIS W. HEWETT, AND GREGORY F. SIMONSON

Plasma Physics Research Institute and D Division, Lawrence Livermore National Laboratory, Livermore, California 94550

Received November 16, 1992; revised August 13, 1993

The finite electron mass streamlined Darwin field (SDF) model is derived for a quasineutral plasma and contrasted to the SDF model for a nonneutral plasma. Because the Darwin model is used, the Courant numerical stability condition $c\,\Delta t/\Delta x < 1$ is avoided. In a quasineutral plasma, the $\omega_{pe}\Delta t < 2$ stability condition and the $\Delta x/\lambda_{De} < 1$ accuracy condition are avoided by the use of a quasineutral Poisson equation. A fast coupled-elliptic solution technique, found to work extremely well with the nonneutral SDF model, also works well with the quasineutral SDF model. Because of the similarity of the field equations for a nonneutral and a quasineutral plasma, it may be possible to simulate a plasma with both nonneutral and quasineutral regions using a single SDF solver.

1. INTRODUCTION

The Darwin or magnetoinductive approximation to Maxwell's equations in a plasma allows solutions that retain the electrostatic, magnetostatic, and inductive electric fields without the time resolution of fully electromagnetic modes. Under this approximation, the hyperbolic Maxwell's equations become the elliptic Darwin equations. Since fully electromagnetic modes are not resolved, the Courant stability condition $c\,\Delta t/\Delta x < 1$, required for the time explicit numerical solution of Maxwell's equations, is avoided.

While it is also possible to solve Maxwell's equations with a time implicit numerical solution, there may be problems of interest in which a Darwin model is preferable. For example, if full EM wave propagation is not needed, the nonphysical dissipation due to implicit differencing of Maxwell's equations would make the Darwin model more accurate [1]. An implicit EM code can also be used to numerically damp plasma oscillations, but $v_{te}\,\Delta t/\Delta x \sim 0.3$ must be maintained for energy conservation [2]. Recently, it has been shown that a method based on guiding center electrons greatly improves energy conservation in implicit schemes [3]. However, this method cannot be used for simulations in which electron cyclotron physics must be retained while electron plasma oscillations can be eliminated, e.g., ECR plasma processing chambers with typical parameters such that $\omega_{pe} \sim 4\omega_{ce}$. We suspect that the Darwin model with quasineutrality included to remove the same scales as implicit simulation may not require the same care in choosing Δt and Δx for many problems.

A new way to formulate the Darwin model in a set of coupled equations has resulted in fewer boundary condition difficulties [4]. Recently, the dynamic ADI (DADI) method for elliptic equations has been successfully applied to these coupled equations [5] resulting in a large reduction in CPU time compared to previous iterative techniques. The nonneutral SDF model has already been used to simulate the MIRRORTRON accelerator [6]. For problems in which space charge waves as well as EM propagation need not be resolved, Hewett and Nielson [7] combined the traditional Darwin model with a quasineutral model to eliminate the $\omega_{pe}\Delta t < 2$ stability condition and the $\Delta x/\lambda_{De} < 1$ accuracy condition as well as the $c\,\Delta t/\Delta x < 1$ stability condition. The key result of the present paper is that the quasineutral equations can also be combined with the new Darwin formulation and DADI can still be applied to the resulting equations.

The quasineutral model will have applications in plasma simulation of high altitude atmospheric disturbances if finite electron mass effects are of interest, e.g., if lower hybrid waves are important. Since the nonneutral and quasineutral SDF equations are so similar, a combined model to treat a plasma with a quasineutral bulk and nonneutral sheath may be possible. A detailed treatment of both plasma regions may be important for plasma processing inductive source simulations.

The plan of this paper is as follows. In Section 2, the quasineutral Darwin model is reviewed. In Section 3, the quasineutral SDF model will be derived and contrasted to the nonneutral SDF model and the choice of DADI will be discussed. In Section 4, some boundary condition issues will be discussed. In Section 5, results for the quasineutral tests will be presented. In Section 6, some concluding remarks concerning merging of the quasineutral and nonneutral models will be made.

0021-9991/94 $6.00

2. BASIC EQUATIONS FOR THE QUASINEUTRAL DARWIN MODEL

For completeness, we give a very cursory derivation of the traditional Darwin model–details can be found in several previous papers [8, 4, 5, 7]. Readers already familar with the quasineutral Darwin model may only want to refer to this section when reading the derivation presented in Section 3. Before starting, we first define the notation of vector decomposition. A vector has a curl-free or irrotational part and a divergence-free or solenoidal part,

$$\mathbf{V} = \mathbf{V}^{\mathrm{IRR}} + \mathbf{V}^{\mathrm{SOL}}, \tag{1}$$

where $\nabla \times \mathbf{V}^{\mathrm{IRR}} = 0$ and $\nabla \cdot \mathbf{V}^{\mathrm{SOL}} = 0$. To solve for $\mathbf{V}^{\mathrm{IRR}} = -\nabla p$ with $\mathbf{V}$ given, take the divergence of Eq. (1). Then

$$\nabla^2 p = -\nabla \cdot \mathbf{V}, \tag{2}$$

where p is the potential. Boundary conditions on p make the decomposition unique.

Maxwell's curl equations including plasma sources are

$$\partial_t \mathbf{B} = -\nabla \times \mathbf{E}, \tag{3}$$

$$\partial_t \mathbf{E} = c^2 \nabla \times \mathbf{B} - c^2 \mu_0 \mathbf{J}. \tag{4}$$

Since $\nabla \cdot \mathbf{B} = 0$, $\mathbf{B}$ is divergence-free or purely solenoidal. Applying Eq. (1) to $\mathbf{E}$ and $\mathbf{J}$ and substituting into Eqs. (3) and (4) gives

$$\partial_t \mathbf{B} = -\nabla \times \mathbf{E}^{\mathrm{SOL}}, \tag{5}$$

$$\partial_t \mathbf{E}^{\mathrm{SOL}} + \partial_t \mathbf{E}^{\mathrm{IRR}} = c^2 \nabla \times \mathbf{B} - c^2 \mu_0 \mathbf{J}^{\mathrm{SOL}} - c^2 \mu_0 \mathbf{J}^{\mathrm{IRR}}. \tag{6}$$

Taking the curl of Eq. (6) and substituting Eq. (5) would result in a wave equation that supports fully electromagnetic modes traveling at the speed of light. It is these waves that require the numerical stability condition $c\,\Delta t/\Delta x < 1$ in explicit codes. To eliminate fully electromagnetic modes, set $\partial_t \mathbf{E}^{\mathrm{SOL}} = 0$. This is the key assumption in the Darwin model; it eliminates retardation effects and thus eliminates purely electromagnetic modes [8]. After this step, one can separate Eq. (6) into irrotational and solenoidal parts,

$$\partial_t \mathbf{E}^{\mathrm{IRR}} + \varepsilon_0^{-1} \mathbf{J}^{\mathrm{IRR}} = 0, \tag{7}$$

$$\nabla \times \mathbf{B} = \mu_0 \mathbf{J}^{\mathrm{SOL}}. \tag{8}$$

Equations (5) and (8) constitute an elliptic set of equations for $\mathbf{B}$ and $\mathbf{E}^{\mathrm{SOL}}$. To see how this is so, first substitute the vector potential $\mathbf{B} = \nabla \times \mathbf{A}$ into Eq. (8) and use the vector identity $\nabla \times \nabla \times \mathbf{A} = \nabla(\nabla \cdot \mathbf{A}) - \nabla^2 \mathbf{A}$. The Coulomb gauge $\nabla \cdot \mathbf{A} = 0$ is chosen to keep the left-hand side of Eq. (8) irrotational. With the Coulomb gauge, one obtains

$$\nabla^2 \mathbf{A} = -\mu_0 \mathbf{J}^{\mathrm{SOL}}. \tag{9}$$

Next, take the curl of Eq. (5), substitute Eq. (8), and use the vector identity $\nabla \times \nabla \times \mathbf{E}^{\mathrm{SOL}} = \nabla(\nabla \cdot \mathbf{E}^{\mathrm{SOL}}) - \nabla^2 \mathbf{E}^{\mathrm{SOL}}$. Note that $\nabla \cdot \mathbf{E}^{\mathrm{SOL}} = 0$ by definition. With this definition, one obtains

$$\nabla^2 \mathbf{E}^{\mathrm{SOL}} = \mu_0 \partial_t \mathbf{J}^{\mathrm{SOL}}. \tag{10}$$

Next, one could take the divergence of Eq. (7), substitute the charge continuity equation, and use the definition $\mathbf{E}^{\mathrm{IRR}} = -\nabla \phi$ to obtain the Poisson equation. Under quasineutrality, $n_e = n_i$ and the Poisson equation cannot be used to find ϕ. However, $\mathbf{E}^{\mathrm{IRR}} \neq 0$ as can be seen with an elementary derivation of ion acoustic waves [9]. Therefore, an equation must be derived for $\mathbf{E}^{\mathrm{IRR}}$ that is appropriate for the quasineutral limit. Quasineutrality also implies that $\mathbf{J}$ should be purely solenoidal but numerical or boundary errors can lead to some $\mathbf{J}^{\mathrm{IRR}}$. Hence $\mathbf{J}^{\mathrm{SOL}}$ is explicitly written in Eqs. (9) and (10) as a reminder that something must be done to make sure $\mathbf{J}$ does not develop an irrotational part in a quasineutral plasma.

Following Hewett and Nielson [7], the quasineutral Poisson equation is derived from the sum of the momentum equations

$$\partial_t n_i \mathbf{U}_i + \nabla \cdot n_i \mathbf{U}_i \mathbf{U}_i = (e/m_i)\, n_i [\mathbf{E} + \mathbf{U}_i \times \mathbf{B}] - \nabla n_i T_i / m_i, \tag{11}$$

for the ions and

$$\partial_t n_i \mathbf{U}_e + \nabla \cdot n_i \mathbf{U}_e \mathbf{U}_e = -(e/m_e)\, n_i [\mathbf{E} + \mathbf{U}_e \times \mathbf{B}] - \nabla n_i T_e / m_e, \tag{12}$$

for the electrons. Note that for simplicity, the collisional terms are not written and one singly charged ion species is used; $n_e = n_i$ is explicitly included. Multiplying Eq. (11) by $e\mu_0$ and Eq. (12) by $-e\mu_0$ and adding the results gives

$$\mu_0 \partial_t \mathbf{J} = \mu \mathbf{E} + \mathbf{Q}, \tag{13}$$

where

$$\mu = \mu_0 [(e^2/m_e) + (e^2/m_i)]\, n_i$$

and

$$\mathbf{Q} = \mu_0 [(e/m_i)\, \mathbf{J}_i \times \mathbf{B} - (e/m_i)\, \nabla n_i T_i - e \nabla \cdot n_i \mathbf{U}_i \mathbf{U}_i - (e/m_e)\, \mathbf{J}_e \times \mathbf{B} + (e/m_e)\, \nabla n_i T_e + e \nabla \cdot n_i \mathbf{U}_e \mathbf{U}_e].$$

From the sum of the continuity equations and $n_e = n_i$, one obtains the quasineutrality condition

$$\nabla \cdot \mathbf{J} = 0. \tag{14}$$

After taking the divergence of Eq. (13) and using Eq. (14) and the definitions $\mathbf{E} = \mathbf{E}^{\mathrm{SOL}} + \mathbf{E}^{\mathrm{IRR}}$, $\mathbf{E}^{\mathrm{IRR}} = -\nabla\phi$, one obtains the quasineutral Poisson equation

$$\nabla \cdot \mu \nabla\phi = \nabla \cdot \mu \mathbf{E}^{\mathrm{SOL}} + \nabla \cdot \mathbf{Q}. \tag{15}$$

Finally, substituting Eq. (13) into Eq. (10) and noting $\partial_t \mathbf{J}^{\mathrm{SOL}} = [\partial_t \mathbf{J}]^{\mathrm{SOL}}$ because ∂_t commutes with both $\nabla\cdot$ and $\nabla\times$, one obtains

$$\nabla^2 \mathbf{E}^{\mathrm{SOL}} = [\mu \mathbf{E} + \mathbf{Q}]^{\mathrm{SOL}}. \tag{16}$$

To summarize, if given appropriate boundary conditions and methods to advance the plasma fluid quantities to the current time level, one could solve Eq. (9), use $\mathbf{B} = \nabla \times \mathbf{A}$ to obtain $\mathbf{B}$, solve Eqs. (15) and (16), and then use $\mathbf{E} = \mathbf{E}^{\mathrm{SOL}} - \nabla\phi$ to obtain $\mathbf{E}$.

Historically, this model has been used for microturbulence studies. These simulations concentrated on localized regions near the plasma boundary. One would like to extend the model to simulate entire plasma regions as is done with zero electron mass Darwin (ZEM) models [10–12].

ZEM models are often set up to model vacuum regions as well as plasma regions. To differentiate between a vacuum cell and a plasma cell, a cutoff density, usually a few percent of the maximum plasma density, is used. If the density in a given cell region is less than the cutoff density, the cell is declared to be a vacuum cell. In the vacuum cells, $\nabla^2 \mathbf{A} = 0$ and $\nabla^2 \mathbf{E} = 0$ are solved instead of the ZEM field equations. The finite cutoff is necessary or the Alfvén wave Courant condition $v_A \Delta t/\Delta x < 1$ would be violated. These ideas are presented in more detail in papers by Hewett and Harned [11, 12] and can also be applied to our model.

Solving Eq. (16) is difficult. Let $\mathbf{S} = \mathbf{Q} + \mu \mathbf{E}$. Then, Eqs. (1) and (2) for the right-hand side decomposition of Eq. (16) give $\nabla^2 \mathbf{E}^{\mathrm{SOL}} = \mathbf{S}^{\mathrm{SOL}} = \mathbf{S} + \nabla s$, where $\nabla^2 s = -\nabla \cdot \mathbf{S}$. Boundary conditions for s are not obvious. Furthermore, if the right-hand side decomposition is done perfectly, the divergence of Eq. (16) gives $\nabla^2[\nabla \cdot \mathbf{E}^{\mathrm{SOL}}] = 0$ but $\nabla \cdot \mathbf{E}^{\mathrm{SOL}} = 0$ is guaranteed to be numerically preserved only if $\nabla \cdot \mathbf{E}^{\mathrm{SOL}} = 0$ is forced on the boundary. Since such control can be difficult to enforce, $\nabla \cdot \mathbf{E}^{\mathrm{SOL}} = 0$ must be guaranteed by numerically removing the part that has finite divergence by divergence cleaning. Part of the motivation for the nonneutral SDF model is to avoid these difficulties. We take a similar approach with the quasineutral model.

3. STREAMLINED EQUATIONS FOR THE QUASINEUTRAL MODEL

A more practical solution procedure for the nonneutral SDF was given by Hewett and Boyd [4]. They found that perfect decomposition was not only impossible numerically but also not necessary for certain arrangements of the equations. For example, if one just solves

$$\nabla^2 \mathbf{A} = -\mu_0 \mathbf{J}, \tag{17}$$

instead of Eq. (9), $\mathbf{A}$ will have spurious irrotational terms. These terms will cancel when $\nabla \times \mathbf{A}$ is used to obtain $\mathbf{B}$ assuming the finite differencing ensures $\nabla \cdot \nabla \times = 0$.

One may be tempted to use another simple argument to streamline Eq. (16). That is, since Eq. (16) must be solved in conjunction with Eq. (15), the right-hand side of Eq. (16) is automatically guaranteed to be divergence-free since the solution of Eq. (15) forces $\nabla \cdot \mathbf{J} = 0$ via the derivation of Eq. (15) from Eq. (14). Although this is true, one is again bedeviled by $\nabla \cdot \mathbf{E}^{\mathrm{SOL}} = 0$ everywhere only if $\nabla \cdot \mathbf{E}^{\mathrm{SOL}} = 0$ is forced on the boundary. One is forced to do divergence cleaning, but fortunately, the divergence cleaning process itself can be incorporated directly into the solution method.

Letting $\mathbf{F}$ be the unclean version of $\mathbf{E}^{\mathrm{SOL}}$, Eq. (16) without the RHS decomposition becomes

$$\nabla^2 \mathbf{F} = \mu(\mathbf{E}^{\mathrm{SOL}} - \nabla\phi) + \mathbf{Q}, \tag{18}$$

where $\mathbf{E} = \mathbf{E}^{\mathrm{SOL}} - \nabla\phi$ has been used. To clean $\mathbf{F}$, one takes $\mathbf{F} = \mathbf{E}^{\mathrm{SOL}} - \nabla\psi$. That is, the solution to Eq. (18) is made up of the wanted quantity $\mathbf{E}^{\mathrm{SOL}}$ and an unwanted quantity due to $\nabla \cdot \mathbf{E}^{\mathrm{SOL}} \neq 0$ numerically. Solving for $\mathbf{E}^{\mathrm{SOL}}$ gives

$$\mathbf{E}^{\mathrm{SOL}} = \mathbf{F} + \nabla\psi. \tag{19}$$

Substituting Eq. (19) into Eq. (18) gives

$$\nabla^2 \mathbf{F} - \mu \mathbf{F} = \mu(\nabla\psi - \nabla\phi) + \mathbf{Q}. \tag{20}$$

An equation for ψ is obtained by taking the divergence of Eq. (19) and using the requirement $\nabla \cdot \mathbf{E}^{\mathrm{SOL}} = 0$. The result is

$$\nabla^2 \psi = -\nabla \cdot \mathbf{F}. \tag{21}$$

Next, Eq. (19) is substituted into Eq. (15) to give

$$\nabla \cdot \mu \nabla\phi = \nabla \cdot \mu(\mathbf{F} + \nabla\psi) + \nabla \cdot \mathbf{Q}. \tag{22}$$

Equations (20)–(22) form a complete set of equations for $\mathbf{E}$, where

$$\mathbf{E} = \mathbf{F} + \nabla\psi - \nabla\phi. \tag{23}$$

This set of equations can be reduced by defining $\tilde{\phi} = \phi - \psi$. Equation (20) becomes

$$\nabla^2 \mathbf{F} - \mu \mathbf{F} = \mathbf{Q} - \mu \nabla \tilde{\phi}. \tag{24}$$

Equation (22) becomes

$$\nabla \cdot \mu \nabla \tilde{\phi} = \nabla \cdot \mathbf{Q} + \nabla \cdot \mu \mathbf{F}. \tag{25}$$

Equation (23) becomes

$$\mathbf{E} = \mathbf{F} - \nabla \tilde{\phi}. \tag{26}$$

Equations (24)–(26) can be used to determine a quasineutral **E**. Equation (21) is never solved. Equation (21) guarantees $\nabla \cdot \mathbf{E}^{\mathrm{SOL}} = 0$ but $\mathbf{E}^{\mathrm{SOL}}$ is not used to determine **E**. In other words, the problem of enforcing $\nabla \cdot \mathbf{E}^{\mathrm{SOL}} = 0$ is circumvented by the redefinition of potentials to include the divergence cleaning error and the error cancels when **E** is formed at the end of the calculation. To check if ϕ can be recovered, one can iterate Eqs. (24) and (25) to convergence, then solve Eq. (21) for ψ, and finally calculate $\phi = \tilde{\phi} + \psi$. The iteration is allowed to select a gauge $\psi \neq 0$, but as will be demonstrated, the correct solutions for **E** and ϕ are always returned.

The vacuum analogues of Eqs. (24) and (25) are

$$\nabla^2 \mathbf{F} = 0 \tag{27}$$

and

$$\nabla^2 \tilde{\phi} = \nabla \cdot \mathbf{F}. \tag{28}$$

This guarantees $\nabla \cdot \mathbf{E} = 0$ in the vacuum. A cutoff switch could be used to solve Eqs. (24) and (25) in a plasma region and Eqs. (27) and (28) in a vacuum region while using the same numerical technique to solve either set of equations.

The nonneutral SDF model is derived from equations similar to those outlined in Section 2. In fact, the main physics difference is that the Poisson equation replaces the quasineutral Poisson equation. The streamlining of the inductive electric field equation is accomplished by adding terms to both sides of Eq. (10) to compensate for not doing the right-hand side decomposition [5]. The potential ψ then contains a physical quantity and is not just a product of divergence cleaning as in the quasineutral case. Now if one again uses $\tilde{\phi} = \phi - \psi$, the nonneutral SDF model becomes

$$\nabla^2 \mathbf{F} - \mu \mathbf{F} = \mathbf{Q} - \mu \nabla \tilde{\phi}, \tag{29}$$

$$\nabla^2 \tilde{\phi} = -\rho/\varepsilon_0 + \nabla \cdot \mathbf{F}, \tag{30}$$

and

$$\mathbf{E} = \mathbf{F} - \nabla \tilde{\phi}. \tag{31}$$

These equations are mathematically similar to Eqs. (24)–(26) and form a more compact version of the nonneutral SDF model.

To solve Eqs. (24) and (25) we use the DADI method applied to coupled elliptic equations. DADI works as follows [13, 5]. An artificial time dependence is added to convert the coupled elliptic equations into parabolic form, then noniterative ADI is used to advance the "parabolic" equations in "time". A dynamic time step size changer is then implemented to speed up convergence to the time asymptotic state which is the solution of the original elliptic equations.

Previous attempts to solve the coupled nonneutral SDF equations using Picard iteration were slow to converge [4]. Application of a rapid elliptic solver (FFT or cyclic reduction) would reduce computer time to solve each equation individually but would not reduce the number of iterations required to solve the coupled set. Furthermore, rapid elliptic solvers require the equation to be analytically separable. With the quasineutral Poisson equation, separability is impossible. One must solve the finite difference version of the equations with a direct matrix inversion method such as a conjugate gradient method or with an iterative method such as ADI.

A thorough comparison between the DADI solver and the BCG solver as applied to the nonneutral SDF model is provided in Hewett, Larson, and Doss [5]. In that paper, DADI was found to give superior performance in solving the equations. Even for problems that took many iterations to get small residuals, DADI fared better. We assume similar performance for the quasineutral SDF equations because this set of equations is mathematically similar to the nonneutral SDF equations.

4. BOUNDARY CONDITION CONSIDERATIONS

In the test cases for the solution of Eqs. (24)–(26), periodic boundaries in y and a known **E** in x will be used. For this case, boundary conditions will be illustrated in detail. A conducting wall boundary condition will also be described.

Consider the left boundary at $x = 0$. Equation (26) gives

$$\mathbf{F}_x(0, y) = \mathbf{E}_x(0, y) + \partial_x \tilde{\phi}(0, y), \tag{32}$$

$$\mathbf{F}_y(0, y) = \mathbf{E}_y(0, y) + \partial_y \tilde{\phi}(0, y). \tag{33}$$

As in the nonneutral SDF model, the boundary conditions for $\tilde{\phi}$ may be chosen arbitrarily. For example, one can have Dirichlet zero, i.e., $\tilde{\phi}(0, y) = 0$ or Neumann zero, i.e.,

$\partial_x \tilde{\phi}(0, y) = 0$. If one allows order Δx accurate finite difference equations on the boundary, then

$$\mathbf{F}_x(0, y) = \mathbf{E}_x(0, y) + (1 - \beta) \times [\tilde{\phi}(\Delta x, y) - \tilde{\phi}(0, y)]/\Delta x, \quad (34)$$

$$\mathbf{F}_y(0, y) = \mathbf{E}_y(0, y) + 0.5\beta \times [\tilde{\phi}(0, y + \Delta y) - \tilde{\phi}(0, y - \Delta y)]/\Delta y, \quad (35)$$

and for $\tilde{\phi}$,

$$\tilde{\phi}(0, y) = \beta \tilde{\phi}(\Delta x, y), \quad (36)$$

where $\mathbf{E}(0, y)$ is known and $\beta = 0$ for Dirichlet zero and $\beta = 1$ for Neumann zero. Similar equations can be derived for the right boundary.

It is also possible to construct boundary conditions that are order Δx^2 accurate. Using Neumann zero boundary conditions for $\tilde{\phi}$, Eqs. (34) and (35) with $\beta = 1$ are used for $\mathbf{F}$ boundary conditions. Next, a finite difference version of Eq. (25) is constructed at $x = 0$. For order Δx^2 accuracy, central differencing is used. Values for μ, $\mathbf{Q}_x$, and $\mathbf{F}_x$ at $x = -\Delta x$ are therefore needed; μ and $\mathbf{Q}_x$ can only be obtained from a projection; i.e.,

$$\mu(-\Delta x, y) = 2\mu(0, y) - \mu(\Delta x, y), \quad (37)$$

and similarly for $\mathbf{Q}_x$. For $\mathbf{F}_x$ at $x = -\Delta x$, the x component of Eq. (24) is used. Also using $\mathbf{F}_x = \mathbf{E}_x$ and $\partial_x \tilde{\phi} = 0$ at $x = 0$, the x component equation at $x = 0$ is

$$\partial_x^2 \mathbf{F}_x = \mathbf{Q}_x + \mu \mathbf{E}_x - \partial_y^2 \mathbf{E}_x. \quad (38)$$

The finite difference version of Eq. (38) gives

$$\mathbf{F}_x(-\Delta x, y) = 2\mathbf{E}_x(0, y) + \Delta x^2 [\mathbf{Q}_x(0, y) + \mu(0, y)\, \mathbf{E}_x(0, y) - \partial_y^2 \mathbf{E}_x(0, y)] - \mathbf{F}_x(\Delta x, y). \quad (39)$$

Finally, the finite difference version of Neumann zero, $\tilde{\phi}(-\Delta x, y) = \tilde{\phi}(\Delta x, y)$, is used in Eq. (25) at $x = 0$. Again, similar equations can be derived for the right boundary.

For an actual problem, consider a vacuum region touching a perfectly conducting wall. If the wall is located at $x = 0$ and runs along y, the physical boundary conditions are $\mathbf{E}_y(0, y) = 0$ and $\partial_x \mathbf{E}_x(0, y) = 0$. This is consistent with requiring $\nabla \cdot \mathbf{E} = 0$ in a vacuum and at the wall. If boundary conditions in $\mathbf{F}$ are chosen to match those of $\mathbf{E}$, the x component of Eq. (27) is solved with a Neumann zero boundary condition at $x = 0$ and the y component of Eq. (27) is solved with a Dirichlet zero boundary condition at $x = 0$.

Next, one could choose $\tilde{\phi} = 0$ at $x = 0$ for the boundary condition of Eq. (28). At $x = 0$, Eq. (28) is then reduced to

$$\partial_x^2 \tilde{\phi}(0, y) = 0. \quad (40)$$

Equation (40) is then used to project the value $\tilde{\phi}(-\Delta x, y) = -\tilde{\phi}(\Delta x, y)$. This would then be used to find $\mathbf{E}_x$ via the x component of Eq. (26).

5. RESULTS FOR THE QUASINEUTRAL TEST PROBLEM

To test the two-dimensional DADI solution of the streamlined quasineutral equations for $\mathbf{E}$, a test electric field is chosen of the form

$$\mathbf{E} = [4x(l_x - x)\cos(2\pi y/l_y)/l_x^2, \; 4x(l_x - x)\sin(2\pi y/l_y)/l_x^2, \; 0]. \quad (41)$$

The field is chosen to have an appreciable irrotational part. With $\mathbf{E}$ given one can decompose it to obtain ϕ. Boundary conditions for ϕ are chosen to be periodic in y and Dirichlet constant in x. Next, the curl of Eq. (3) is taken and Eq. (8) is substituted to obtain

$$\mu_0 \partial_t \mathbf{J}^{\mathrm{SOL}} = -\nabla \times \nabla \times \mathbf{E}. \quad (42)$$

If one uses the quasineutral assumption $\mathbf{J}^{\mathrm{SOL}} = \mathbf{J}$, Eq. (13) can be substituted into Eq. (42) to obtain

$$\mathbf{Q} = -\nabla \times \nabla \times \mathbf{E} - \mu \mathbf{E}. \quad (43)$$

With μ picked to be

$$\mu = v(x/l_x + 1 - f \sin(4\pi y/l_y)), \quad (44)$$

where $f = 0$ for a curved μ and $f = 1$ for a ramped μ, Eq. (43) can be used to obtain $\mathbf{Q}$.

With $\mathbf{Q}$ and μ known, Eqs. (24) and (25) are iterated to convergence. The coupled equations are said to converge when the $L2$ norm of the residual, normalized by the $L2$ norm of the source terms $\mathbf{Q}$ and $\nabla \cdot \mathbf{Q}$, is less than a chosen test parameter ε. Once Eqs. (24) and (25) are solved, Eq. (26) is used to obtain $\mathbf{E}_*$ for comparison to the original test field $\mathbf{E}$; $\mathbf{E}_*$ should equal $\mathbf{E}$ within convergence error. Finally, Eq. (21) is solved for ψ. The boundary conditions for ψ are $\psi(0, y) = \phi(0, y) - \tilde{\phi}(0, y)$. Similar boundary conditions are used at $x = l_x$; $\psi + \tilde{\phi}$ should equal ϕ within convergence error. Note that in an actual simulation there is no need to solve Eq. (21).

The physical parameters of the test problem were $l_x = 20$, $l_y = 20$, and $v = 1 \times 10^4$ in arbitrary units. The large value of v was chosen to mimic the small collisionless skin depth in a quasineutral plasma. The numerical parameters were 39 grid points in x and 31 grid points in y. The tests were performed on a CRAY2 machine running UNICOS.

The shape of μ, the x boundary conditions for $\tilde{\phi}$, and the test parameter ε were varied for the test. The y boundary

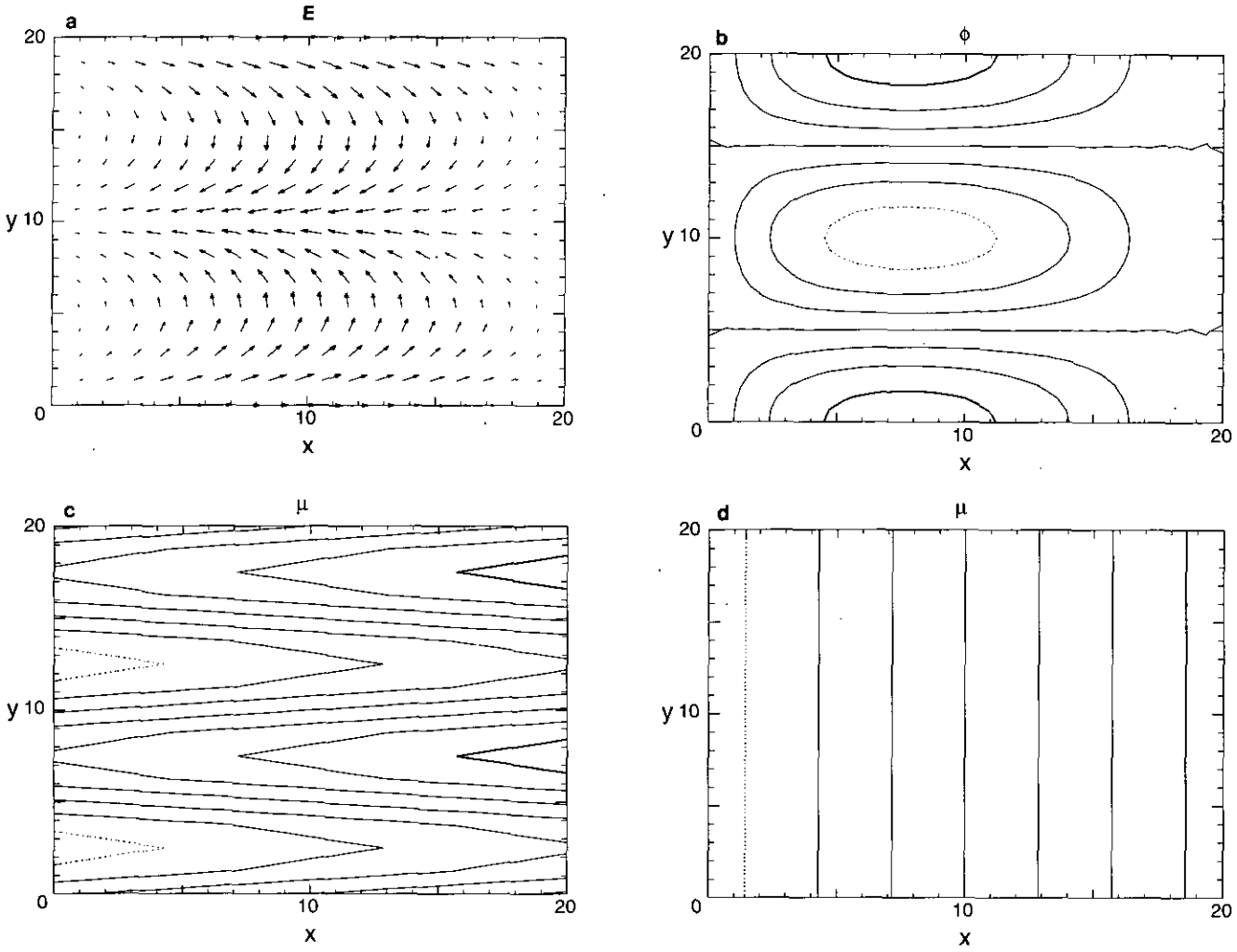

FIG. 1. (a) **E** with longest vector 0.997. (b) ϕ with minimum contour -2.36 and maximum contour 2.36. (c) Curved μ with minimum contour 2.19×10^3 and maximum contour 2.78×10^4. (d) Ramped μ with minimum contour 1.07×10^4 and maximum contour 1.93×10^4. All contour plots have seven equally spaced contours with the minimum contour indicated by the dotted line and the maximum contour indicated by the bold line.

conditions were periodic. Figure 1a shows the chosen **E** with the given parameters. Figure 1b shows the ϕ that results from the decomposition of **E**. Figure 1c shows the curved μ and Fig. 1d shows the ramped μ.

Figures 2, 3, and 4 pertain to a curved μ and $\varepsilon = 10^{-3}$. Figures 2a and 2b are the **F** and $\tilde{\phi}$ solutions with Dirichlet zero x boundary conditions for $\tilde{\phi}$. Figure 2c shows the resulting field $\mathbf{E}_*$ and Fig. 2d shows the error $\mathbf{E} - \mathbf{E}_*$. Figure 2e shows the resulting potential $\phi_* = \tilde{\phi} + \psi$ and Fig. 2f shows the error $\phi - \phi_*$; 83 iterations were required for convergence. Figures 3 show a similar combination for solutions with Neumann zero x boundary conditions for $\tilde{\phi}$; 148 iterations were required for convergence. Figures 4 show a similar combination for solutions with Neumann zero x boundary conditions for $\tilde{\phi}$ and with order Δx^2 accurate differencing on the x boundaries; 551 iterations were required for convergence. Note that the accuracy for x boundary differencing on Figs. 2 and 3 was only order Δx.

The main result of all of these figures is that despite the difference in the choice of the arbitrary boundary condition for $\tilde{\phi}$, the correct solutions for **E** are always returned with 1% or less error and the correct solutions for ϕ are always returned within 2.5% or less error. The topology of the solutions for **F** and especially for $\tilde{\phi}$ change on converting from Dirichlet zero to Neumann zero boundary conditions. No reduction in error is evident from the use of order Δx^2 accurate boundary conditions.

Figures 5 pertain to a ramped μ, $\varepsilon = 10^{-3}$, and Dirichlet zero boundary conditions for $\tilde{\phi}$. Both **E** and ϕ are returned within 1% or less error. Neumann zero, order Δx and Neumann zero, order Δx^2 tests were also done successfully. The Dirichlet zero solution converged in 19 iterations, the

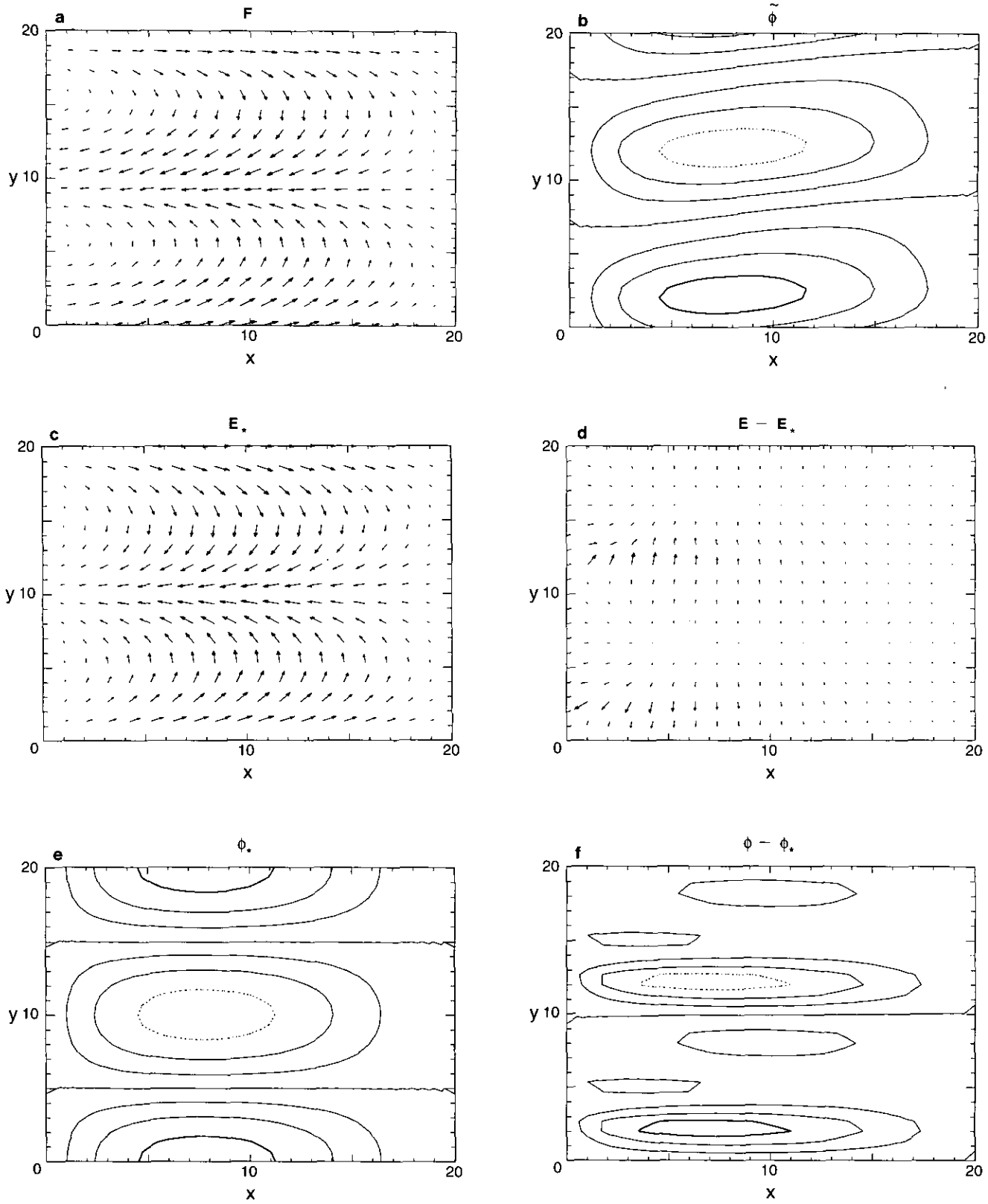

FIG. 2. (a) **F** with longest vector 0.945. (b) $\tilde{\phi}$ with minimum contour at -1.00 and maximum contour at 1.00. (c) $\mathbf{E}_*$ with lonest vector 0.997. (d) $\mathbf{E}-\mathbf{E}_*$ with longest vector 2.48×10^{-3}. (e) ϕ_* with minimum contour -2.36 and maximum contour 2.36. (f) $\phi-\phi_*$ with minimum contour -2.03×10^{-2} and maximum contour 2.03×10^{-2}.

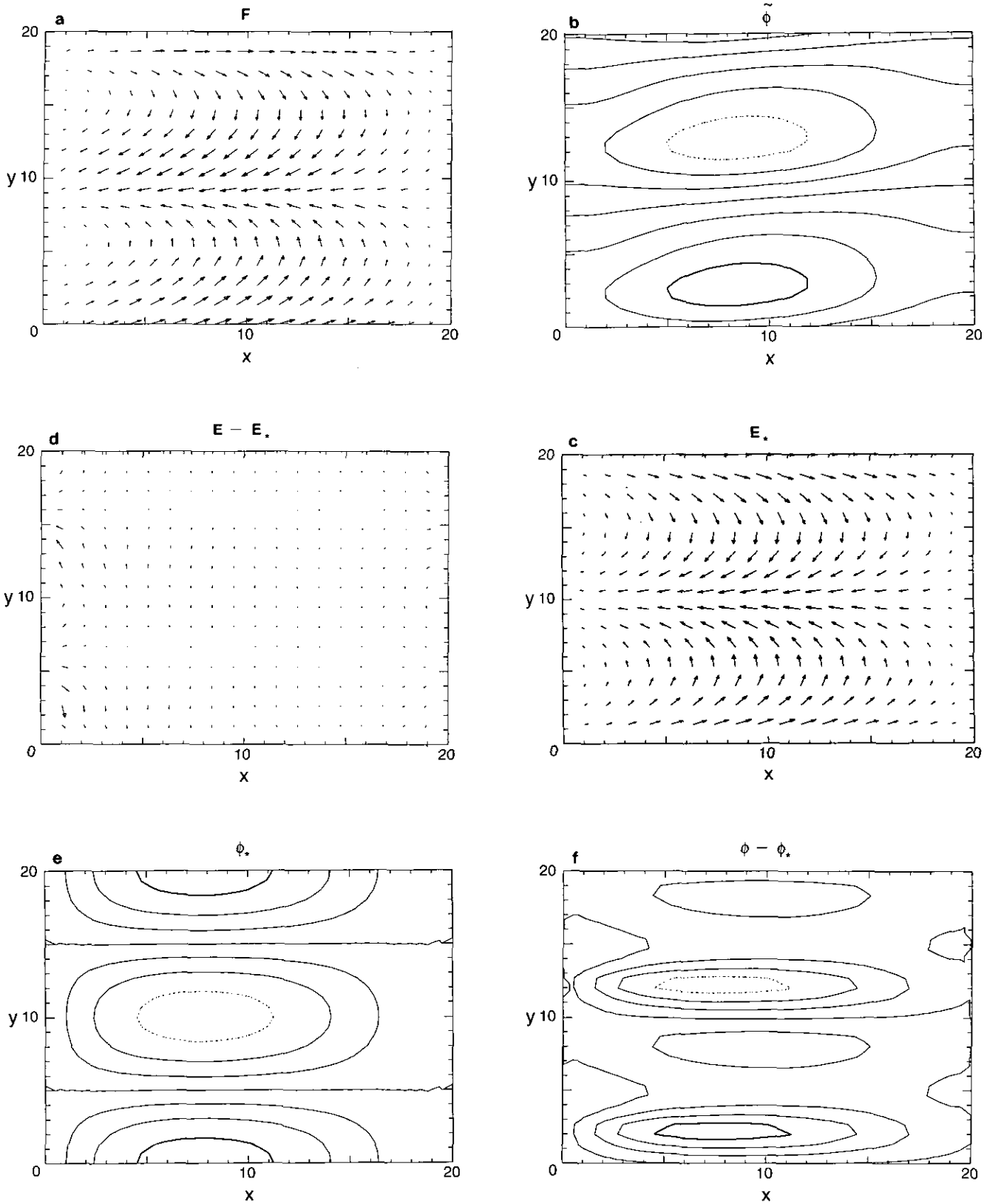

FIG. 3. (a) **F** with longest vector 0.953. (b) $\tilde{\phi}$ with minimum contour -1.15 and maximum contour at 1.15. (c) $\mathbf{E}_*$ with longest vector 0.997. (d) $\mathbf{E}-\mathbf{E}_*$ with longest vector 3.02×10^{-3}. (e) ϕ_* with minimum contour -2.36 and maximum contour 2.36. (f) $\phi-\phi_*$ with minimum contour -2.14×10^{-2} and maximum contour 2.15×10^{-2}.

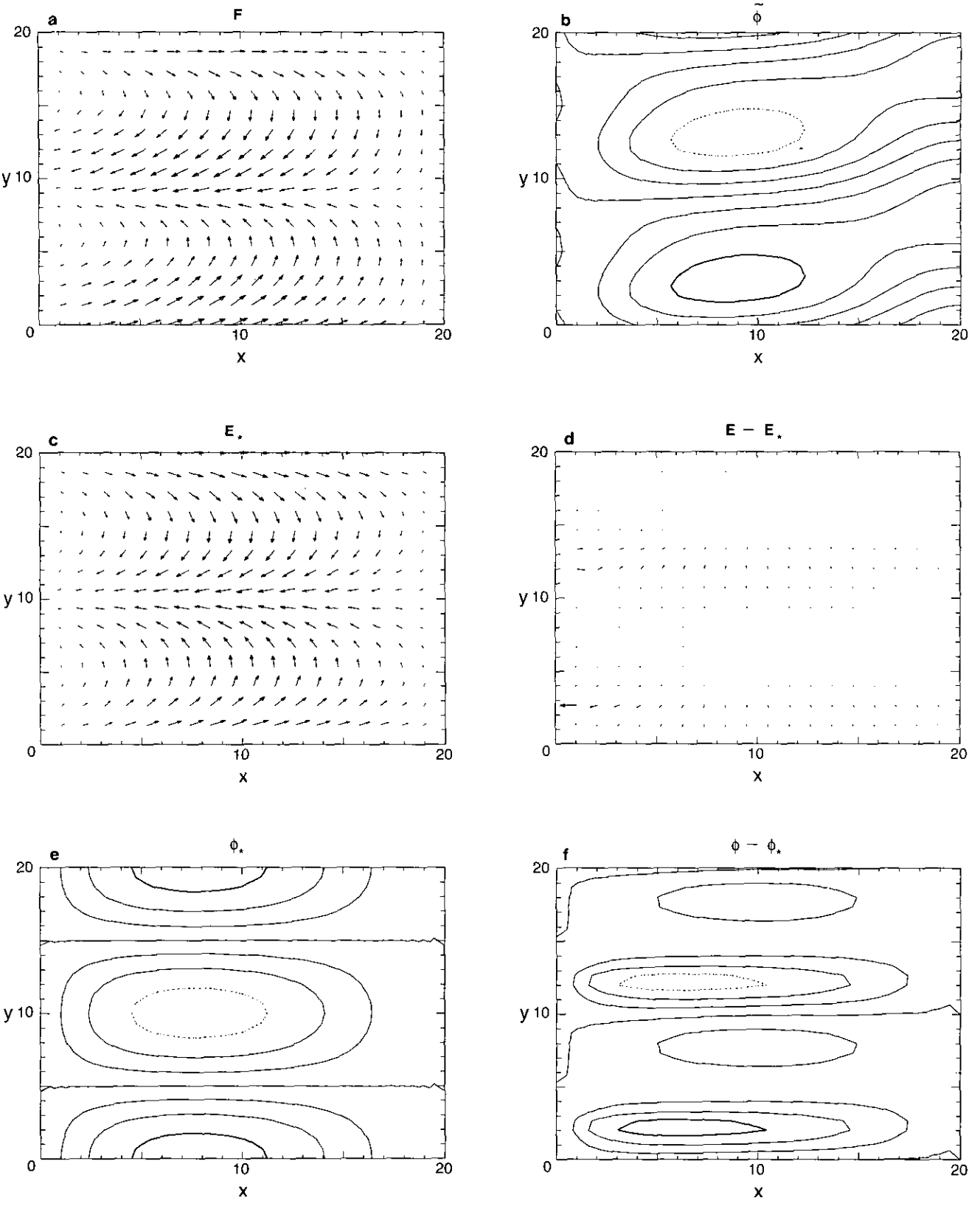

FIG. 4. (a) **F** with longest vector 0.952. (b) $\tilde{\phi}$ with minimum contour at -1.19 and maximum contour at 1.19. (c) $\mathbf{E}_*$ with longest vector 0.997. (d) $\mathbf{E}-\mathbf{E}_*$ with longest vector 2.61×10^{-3}. (e) ϕ_* with minimum contour -2.36 and maximum contour 2.36. (f) $\phi-\phi_*$ with minimum contour -2.33×10^{-2} and maximum contour 2.33×10^{-2}.

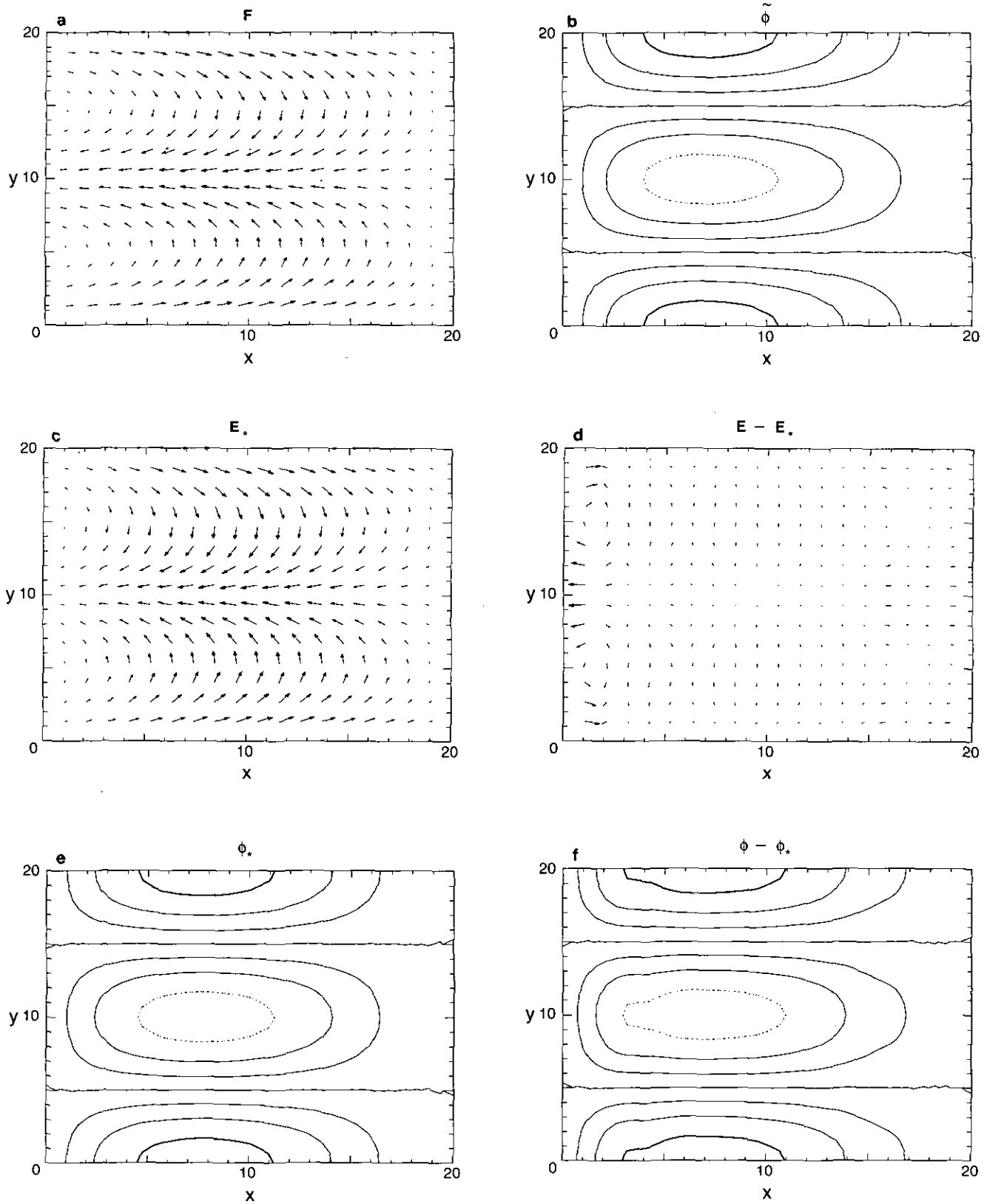

FIG. 5. (a) **F** with longest vector 0.950. (b) $\tilde{\phi}$ with minimum contour at -0.753 and maximum contour at 0.753. (c) $\mathbf{E}_*$ with longest vector 0.997. (d) $\mathbf{E}-\mathbf{E}_*$ with longest vector 1.37×10^{-3}. (e) ϕ_* with minimum contour -2.37 and maximum contour 2.37. (f) $\phi-\phi_*$ with minimum contour -5.37×10^{-3} and maximum contour 5.37×10^{-3}.

Neumann zero solution converged in 45 iterations, and the Neumann zero solution with order Δx^2 boundary differencing converged in 24 iterations. It may be that because $\partial_y \mu = 0$ and the equations take a simpler form, the ramped μ cases converge more quickly.

We have also done cases for

$$\mu = 100(1 + R)(2 - \sin(ky)), \tag{45}$$

for $x < 5$ and $x > 10$ and

$$\mu = 10{,}000(1 + 0.1R)(2 - \sin(ky)), \tag{46}$$

for $5 \leqslant x \leqslant 10$, where R is a random number between zero and one. This μ was chosen to mimic the kind of jagged densities that may be generated in simulations. As expected, both $\mathbf{E}$ and ϕ are returned within 1% or less error. For $\varepsilon = 10^{-3}$, the Dirichlet zero solution converged in 56 iterations, the Neumann zero solution converged in 63 iterations, and the Neumann zero solution with order Δx^2 boundary differencing converged in 56 iterations.

When smaller residuals were chosen, convergence became more difficult. A simple run with a ramped μ and Dirichlet zero boundary conditions at Δx accuracy requires 2508 iterations to converge to $\varepsilon = 10^{-8}$ as opposed to 19 iterations to converge to $\varepsilon = 10^{-3}$ as previously mentioned. For a Dirichlet zero boundary condition and μ from Eqs. (45) and (46), 1070 iterations were required to converge to $\varepsilon = 10^{-5}$.

In all runs, the normalized residual oscillates about a slowly descending envelope. The oscillation in residual suggests there is a wave equation being solved during the iteration in "time." The oscillation may be damped away more rapidly and thus reduce iteration count to convergence if more implicitness is added to DADI. Here, the DADI implicitness is confined to the dependent quantity in the equation, i.e., $\mathbf{F}$ in Eq. (24) and $\tilde{\phi}$ in Eq. (25); $\tilde{\phi}$ in Eq. (24) and $\mathbf{F}$ in Eq. (25) are both lagged in "time." Recently, a new version of DADI for coupled elliptic equations in which the lagging is removed has shown a large reduction in the iteration count and in the overall cpu time to achieve low residuals [14]. With some modification required by the $\nabla \cdot \mu \mathbf{F}$ term in Eq. (25), the new version of the DADI method would be applicable here.

6. CONCLUSION

The quasineutral streamlined Darwin solution in its present form is already applicable to several simulations such as magnetically confined plasmas and magnetospheric plasmas. To make such simulations practical, time step constraints of the form $\omega_{ce} \Delta t < 1$ could be relaxed by an implicit treatment of the magnetic field and fluid equations. Of course, as mentioned in the Introduction, implicit methods may introduce numerical errors and so must always be used carefully.

To apply this solution technique to general plasma processing simulations, we need to complete other developments. For example, a way to couple waveguide or antenna modes into the Darwin equations must be found. Also, we must consider a combined quasineutral and nonneutral simulation. If appropriate simulation boundary conditions and methods to advance the plasma fluid quantities in either a quasineutral or nonneutral region of the plasma are given, a generalized streamlined Darwin model for the electric and magnetic fields can be written. This enables detailed sheath modeling which is not possible if the vacuum equations, Eqs. (27) and (28), are solved in a low density nonneutral region. The equations for the magnetic field remain the same as before, but Eqs. (24) and (25) could be merged with Eqs. (29) and (30) to form a single set of equations that is still amenable to DADI. A switch from fully nonneutral to fully quasineutral solution would have to be devised. One such switch could be based on a comparison of the mesh size to the local Debye length. If the Debye length is poorly resolved, a quasineutral solution could be chosen, whereas if the Debye length is well resolved, a nonneutral solution could be chosen.

ACKNOWLEDGMENTS

We thank Dr. John Ambrosiano for many useful discussions concerning boundary conditions for Darwin models. Work performed under the auspices of the U.S. Department of Energy by the Lawrence Livermore National Laboratory under Contract W-7405-ENG-48.

REFERENCES

1. A. B. Langdon and D. C. Barnes, in *Multiple Time Scales*, edited by B. I. Cohen and J. U. Brackbill (Academic Press, Orlando, FL, 1985), p. 335.
2. B. I. Cohen, A. B. Langdon, D. W. Hewett, and R. J. Procassini, *J. Comput. Phys.* **81**, 151 (1989).
3. M. Tanaka, *J. Comput. Phys.* **107**, 124 (1993).
4. D. W. Hewett and J. K. Boyd, *J. Comput. Phys.* **70**, 166 (1987).
5. D. W. Hewett, D. J. Larson, and S. K. Doss, *J. Comput. Phys.* **101**, 11 (1992).
6. D. J. Larson, Ph. D. Dissertation, University of California, Davis-LLNL, 1992.
7. D. W. Hewett and C. W. Nielson, *J. Comput. Phys.* **29**, 219 (1978).
8. C. W. Nielson and H. R. Lewis, in *Methods in Computational Physics, Vol. 16*, edited by B. Alder, S. Fernbach, M. Rotenberg, and J. Killeen (Academic Press, New York, 1976), p. 367.
9. D. R. Nicholson, *Introduction to Plasma Theory* (Wiley, New York, 1983), p. 138.
10. J. A. Byers, B. I. Cohen, W. C. Condit, and J. D. Hanson, *J. Comput. Phys.* **27**, 476 (1978).
11. D. W. Hewett, *J. Comput. Phys.* **38**, 378 (1980).
12. D. S. Harned, *J. Comput. Phys.* **47**, 452 (1982).
13. S. K. Doss and K. A. Miller, *SIAM J. Numer. Anal.* **16**, 837 (1979).
14. G. DiPeso, D. W. Hewett, D. J. Larson, *Comput. Physics Commun.* **77**, 33 (1993).